Smart Rock Technology for Real-time Monitoring of Bridge Scour and Riprap Effectiveness – Design Guidelines and Visualization Tools (Progress Report No. 4)

Contract No: OASRTRS-14-H-MST
(Missouri University of Science and Technology)

Reporting Period: July 1 – September 30, 2015

PI: Genda Chen

Program Manager: Mr. Caesar Singh

Submission Date: October 15, 2015

TABLE OF CONTENTS

EXECUTIVE SUMMARY

In the fourth quarter of this project, the design of smart rocks (size, density, and internal configurations) was finalized based on the hydraulics, river cross section, and bridge substructure configuration at three bridge sites. The smart rock prototypes were fabricated for deployment. The specially designed test apparatus that facilitates the field tests at bridge sites was manufactured; it can be installed on an open trailer for easy positioning during field demonstration tests. The newly purchased three-axis magnetometer was tested for field operation. Finally, the field demonstration test was carried out at the Waddell Creek Bridge, California.

I - TECHNICAL STATUS

I.1 ACCOMPLISHMENTS BY MILESTONE

In this quarter, the design of smart rocks was updated and the smart rocks were fabricated for the Waddell Creek Bridge, CA, the US 63 Gasconade River Bridge, MO, and the I-44 Roubidoux Creek Bridge, MO, in accordance with the previous deployment plan. The field demonstration test was conducted at the Waddell Creek Bridge, Br. No. 36-0065, CA. Three smart rocks with two stacked magnets each as an automatically pointing to upward system (APUS) were deployed around Abutment 1 and Bent 2. The custom-designed test apparatus was fabricated and used to facilitate the three-dimensional movement of a 3-axis magnetometer around the deployed smart rocks. The 3-axis flux magnetometer sensor head mounted on the test apparatus measured the magnetic field of ambient environment alone or ambient environment plus the deployed smart rocks. To collect ground truth data, a prism was mounted on the apparatus in proximity to the magnetometer sensor and positioned with a total station to survey the three-dimensional coordinates of each measurement point. In addition, a sonar system was attached to a small boat and employed to map the river bed profile around Bent 2. Finally, the localization of smart rocks was performed based on the magnetic field data and measurement point coordinates.

Task 2.1 Final Design of Smart Rocks

A. Size and Density

In order to increase the effective measurement distance for magnetic fields, two stacked magnets (4" in diameter and 4" in total height) or one larger magnet (6" in diameter and 2" in height) were considered as the magnetic core of a smart rock for field deployment. The sizes of inside and outside balls were increased to meet the floating requirement of inside ball with the two stacked magnet inside the outside ball. The diameters 25 cm and 28 cm commercially available for inside and outside balls were selected respectively.

To cast concrete encasement as enclosure of a smart rock, a 14.5 in-diameter standard mold was selected. Substituting this size of smart rock (d=14.5 in. or 36.83 cm) into those incipient motion equations as did in the second progress report yielded the density of smart rocks for three bridge sites:

(1) Highway 1 over Waddell Creek Bridge (Br. No.36-0065)

$$2.286 = \frac{0.052^{1/2}\left(\frac{\rho_s}{1000}-1\right)^{1/2} 0.3683^{1/2} 3.566^{1/6}}{0.03471}, \quad \rho_s = 1215 kg/m^3$$

where d = 0.3683 m for smart rocks based on the required space for magnet embedment;
K_s = 0.052 for fine cobbles from the USGS Scientific Investigations Report 2008-5093;
$S_s = \rho_s/1000$ where ρ_s is the mass density of smart rocks in kg/m^3;
g = 9.81 m/s^2;
V_c = V = 2.286 m/s at Bent 2;
y = 3.566 m at Bent 2;
$n = 0.041 d^{1/6} = 0.03471$.

(2) US 63 Gasconade River Bridge

$$1.218\times1.7=\frac{0.052^{1/2}\left(\frac{\rho_s}{1000}-1\right)^{1/2}0.3683^{1/2}12.192^{1/6}}{0.03471},\quad \rho_s=1117\,kg/m^3$$

where d = 0.3683 m for smart rocks based on the required space for magnet embedment;
K_s = 0.052 for fine cobbles from the USGS Scientific Investigations Report 2008-5093;
$S_s = \rho_s/1000$ where ρ_s is the mass density of smart rocks in kg/m^3;
g = 9.81 m/s^2;
$V_c = V_{average}$ = 1.218 m/s at Bent 4;
y = 12.192 m at Bent 4;
$n = 0.041d^{1/6}$=0.03471.

(3) I-44 Roubidoux Creek Bridge (Bridge No. L0039)

$$0.474\times1.7=\frac{0.052^{1/2}\left(\frac{\rho_s}{1000}-1\right)^{1/2}0.3683^{1/2}5.70^{1/6}}{0.03471},\quad \rho_s=1022\,kg$$

where d = 0.3683 m for smart rocks based on the required space for magnet embedment;
K_s = 0.052 for fine cobbles from the USGS Scientific Investigations Report 2008-5093;
$S_s = \rho_s/1000$ where ρ_s is the mass density of smart rocks in kg/m^3;
g = 9.81 m/s^2;
$V_c = V_{average}$ = 0.474 m/s at Bent 6;
y = 5.70 m at Bent 6;
$n = 0.041d^{1/6}$=0.03471.

Due to variability in hydraulic parameters as a result of potential climate change and the change in river condition, the calculated mass density from the critical velocity should be increased by 1.2 or 1.3 times, depending on the available hydraulic data at bridge sites, in order to prevent the deployed smart rocks from being washed away.

Specifically, for *Highway 1 Waddell Creek Bridge,* a design factor of 1.2 was considered since a detailed 2D hydraulic model was developed by Caltrans to derive the hydraulic parameters at the bridge site. Therefore, the density of smart rocks should be 1.2×1215 = *1458 kg/m^3*. For all other bridges*,* a larger design factor of 1.3 was considered due to insufficient information on the local hydraulic data at these sites. Therefore, the density of smart rocks should be 1.3×1117 = *1452kg/m^3* for *US63 Gasconade River Bridge*, and 1.3×1022 = *1432 kg/m^3* for I-44 *Roubidoux Creek Bridge*. For easy fabrication, the target density of smart rocks was finally taken to be *1495 kg/m^3* for a given diameter of *0.3683 m*.

B. Internal Configuration

The configuration of an APUS smart rock is determined based on the gravity balance as shown in Figures 1 and 2 for two N42 magnets in stack or one N45 magnet, respectively. The magnets are made of rare earth neodymium NdFeB and graded by its maximum energy product. The higher the grade number, the stronger the magnetic field. The maximum residual flux density (Br. Max) of two stacked N42 magnets is 1.32 Tesla. The maximum residual flux density of one N45 magnet is 1.38 Tesla. The two stacked N42 magnets were designed for the Waddell Creek

Bridge and I-44 Roubidoux Creek Bridge while the N45 magnet was developed for the US63 Gasconade River Bridge.

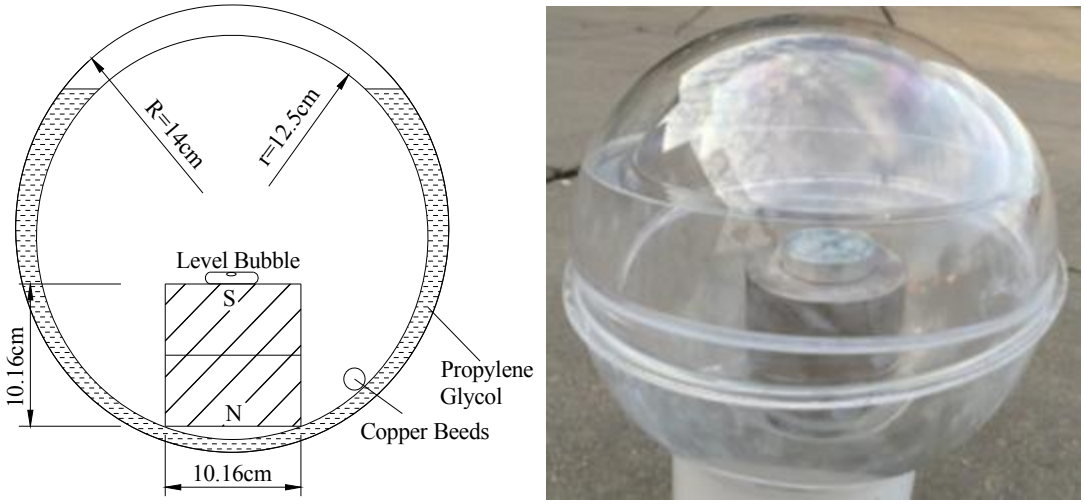

(a) Schematic View (b)Prototype of Smart Rock

Figure 1 APUS Model with Two N42 Magnets

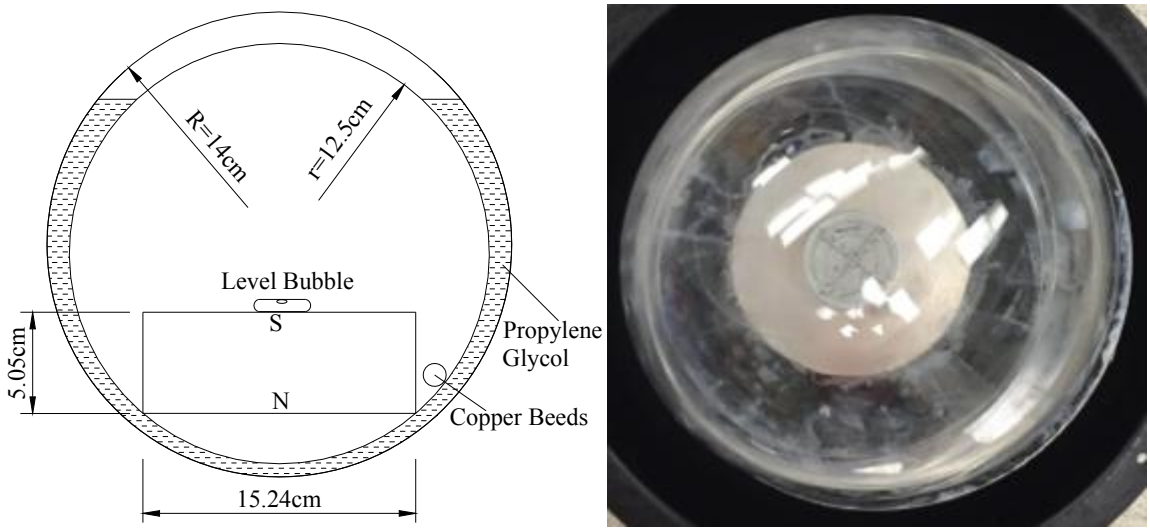

(a) Schematic View (b)Prototype of Smart Rock

Figure 2 APUS Model with One N45 Magnet

Task 2.2 Prototyping of Passive Smart Rocks - Concrete Encasement

For field deployment at bridge sites, each prototype APUS smart rock was cast in a spherical concrete encasement. The smart rock with concrete encasement as schematically shown in Figure 3 was cast in a 36.83cm-diameter mold. The total density of the smart rock is, ρ_s = [$(0.28^3 m^3)$ (850kg/m^3) + ($0.3683^3 m^3$-$0.28^3 m^3$)(2000kg/m^3)] / 0.3683^3 or ρ_s =1495kg/m^3, which is appropriate for all three bridge sites.

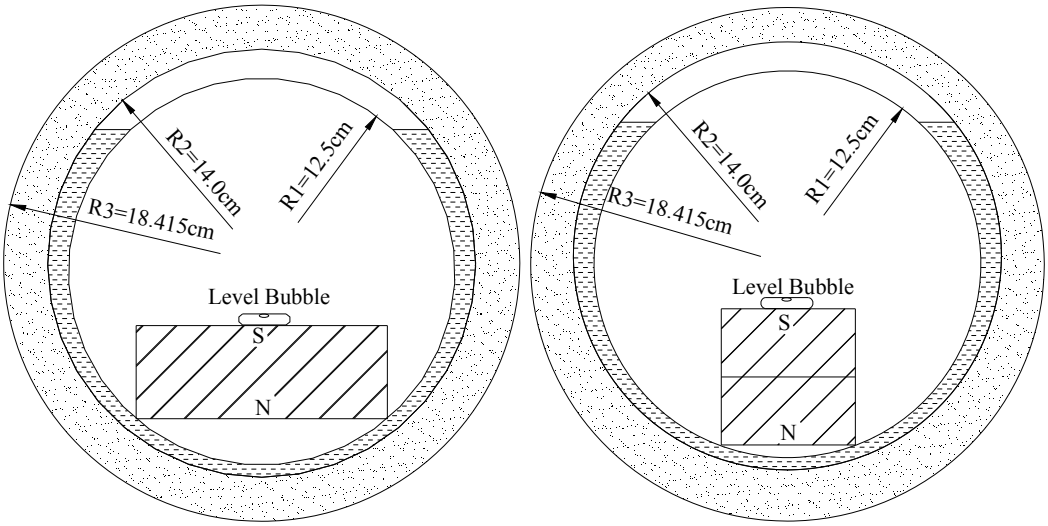

Figure 3 Schematic View of the Concrete Encasement

The mix proportion of concrete was selected to be: water =288 kg/m^3, cement=640 kg/m^3, sand (diameter=4.75 mm)=1023 kg/m^3, fiber=2 kg/m^3 and water reducer admixture=8 kg/m^3. The concrete fiber (FORTA ULTRA-NET) was made of virgin homopolymer polypropylene and came in a collated fibrillated twisted bundle, which is often used to reduce plastic and hardened concrete shrinkage, improve impact strength, and increase fatigue resistance and concrete toughness. A rope across the outside ball and concrete encasement and tied around the stiffener of two halves of the outside ball was used to allow pulling of the smart rock during field deployment and mark the rock location after the deployment. The four-step fabrication process of concrete encasement is shown in Figure 4: 1.) preparing fiber reinforced concrete; 2) pouring a small amount of concrete into the bottom half of a plastic mold, placing and pushing an APUS model into the concrete, and covering the APUS with the top half of the mold; 3) filling the mold with concrete while tapping the mold with a hammer to remove potential air bubbles; and 4) removing the mold once concrete is set in one day and putting the smart rock under water to cure for 14 days.


(a) Prepare Fiber Reinforced Concrete (b) Place an APUS into Concrete and Mold

(c) Fill the Mold with Concrete (d) Cure the Concrete Encasement in Water for 14 Days

Figure 4 Fabrication of Concrete Encasement

Task 3.1 Time- and Event-based Field Measurements

In this task, the field demonstration test was carried out on the deck of HYW1 Waddell Creek Bridge, CA. The river bed profile was mapped by a sonar system. The three smart rocks were deployed around abutment 1 for riprap effectiveness and around bent 2 for bridge scour motoring. The test apparatus with a mounted magnetometer sensor was employed to facilitate measurements of the intensity and direction of the ambient magnetic field and the total field after the smart rocks had been deployed. Finally, the smart rock SR3 was located based on the collected data.

A. Test Setup and Layout

All tests were conducted near south abutment at Bent 1 (Santa Cruz side) and the pier at Bent 2 of the 4-span bridge as shown in Figure 5 (a) and Figure 5(b), respectively. A total station was set near north abutment at Bent 5 on the San Francisco side. The center of the total station was used as the origin of a Cartesian coordinate system XYZ with X-, Y-, and Z- axles defined along the transverse, longitudinal (traffic direction), and vertical upward directions, respectively. Two smart rocks, designed by SR1 and SR2, were deployed on two sides of the Bent 2 in far and near distance, respectively. The third smart rock, SR3 placed in the gap of the riprap rocks around south abutment at Bent 1. The magnetometer sensor mounted on the test apparatus was extended down from the bridge deck for measurement of the ambient magnetic field and the total magnetic field with the smart rocks placed at three locations. Prism 3 mounted below the sensor as shown in Figure 5(c) was used to represent the location of each measurement point. Prism 1 and 2 fixed at two end of the horizontal bar of the test apparatus were employed to ensure the beam indeed horizontal. The measurement points in XOY plane shown in Figure 5(a) were selected as cross points in Mesh 1 for Bent 2 and Mesh 3 for south abutment at Bent 1. Mesh 1 and Mesh 3 for measurement points were then translated to Mesh 2 and Mesh 4 on the bride deck for representative positions of the forklift during tests, as displayed in Figure 5(d). For each point in XOY plane, seven elevations denoted as Z1, Z2, Z3, Z4, Z5, Z6 and Z7 with equal spacing of 0.3 m are positioned for measurements in Z-direction. Therefore, a total measurement point of 112 for SR3 around south abutment at Bent 1 and 140 for SR1 & SR2 around Bent 2 are taken. The

total station set near north abutment at Bent 5 was used to measure the coordinates (location) of three smart rocks and the magnetometer sensor as ground true data.

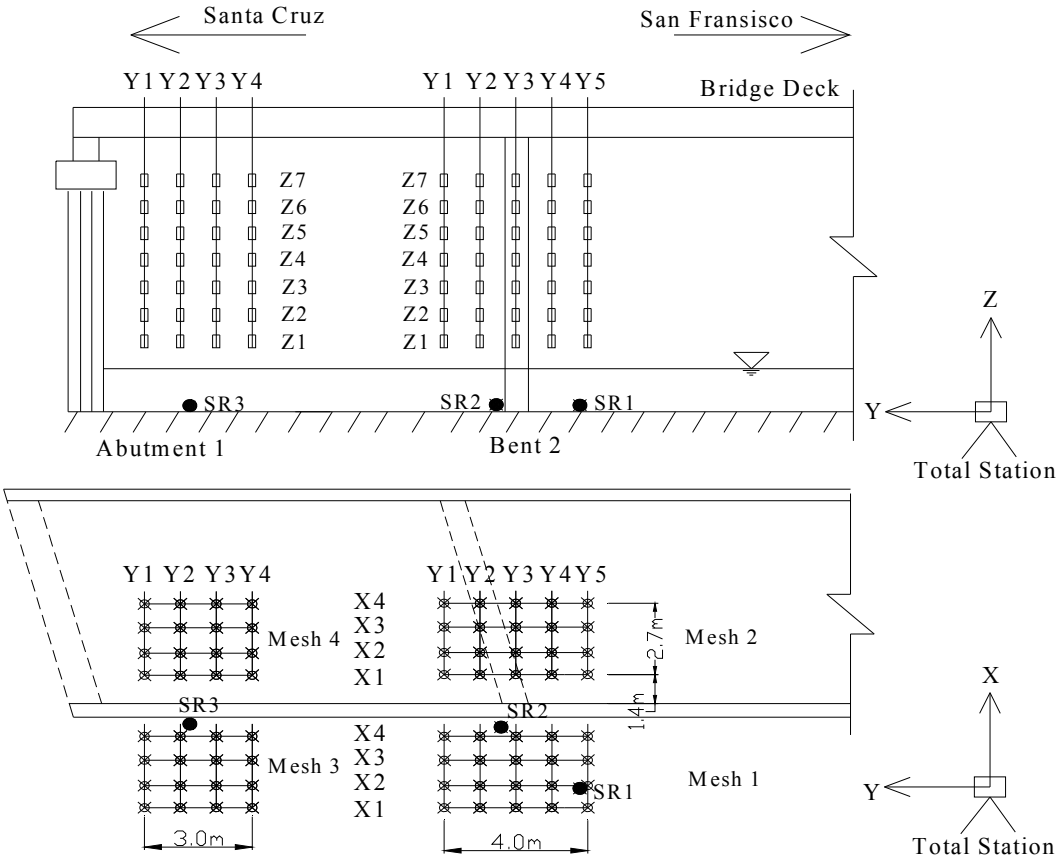

(a) Schematic View of Smart Rocks and Sensor Locations in Plane

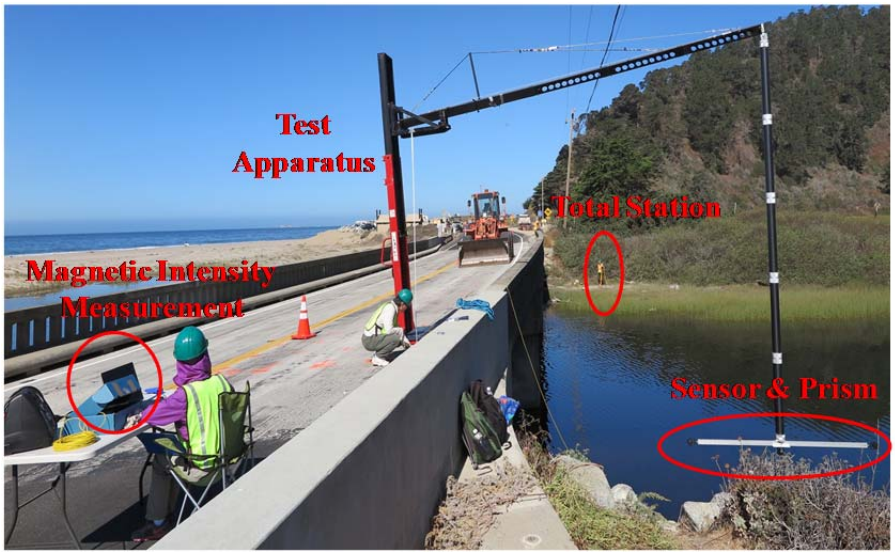

(b) Layout of Whole Measurement System

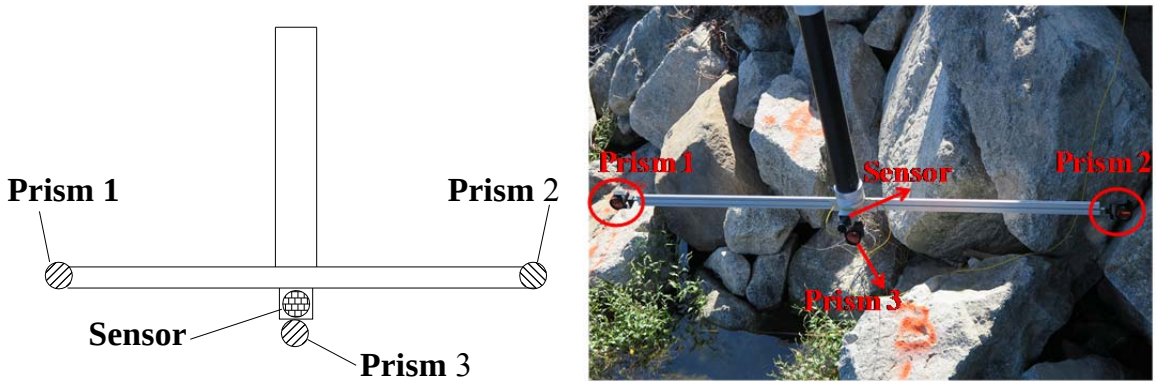

(c) Sensor ang Prism Positions

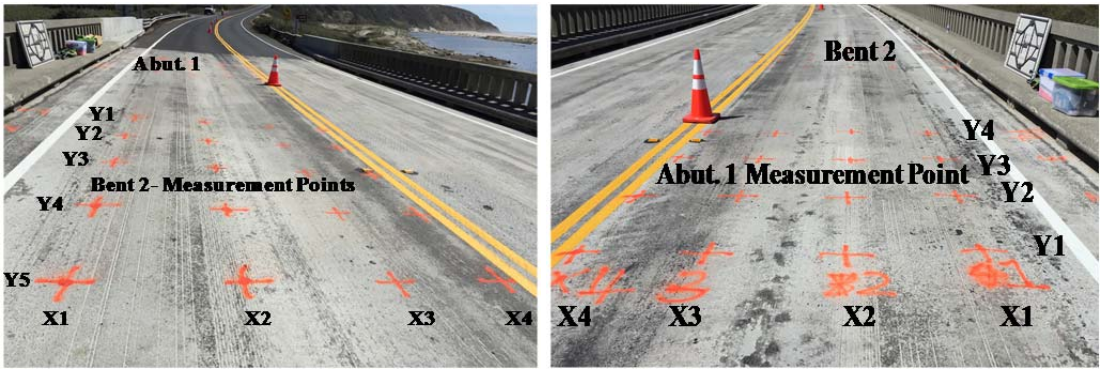

(d) Forklift Position Points

Figure 5 Test Setup at the Waddell Creek Bridge Site

B. Test Procedures

(1) ***Set the XYZ Coordinate System.*** As shown in Figure 6, a permanent Point A on concrete pedestal at the top and upstream/east side of south abutment was selected as the benchmark for this bridge site. The total station was set at Point O on the north end of the bridge such that Y-axis along the traffic (longitudinal) direction to Santa Cruz is parallel to the tangential line of bridge railing closest to Point A, X-axis is perpendicular to the Y-axis and pointing to downstream/west in the horizontal plane, and Z-axis is upward according to the right hand rule. Note that the total station must be in a secure location for easy setup and must be able to view all the measurement points around south abutment and Bent 2.

(2) ***Map the Riverbed Profile.*** The 999ci HD KVD SI Combo/900 Series - Side imaging instrument from Humminbrid shown in Figure 7(a) was used to map the riverbed profile around the studied area. The instrument is based on the sonar mechanism to complete the HD side and down imaging. The included GPS chart plotting with built-in Humminbrid ContourXD map and Ethernet networking capabilities provides the altitude and latitude corresponding to each mapping. As shown in Figure 7(b), the sonar transducer was fixed at the bottom of the boat and operated by one person while the other person ran the boat at certain speed. Several straight paths in transverse and longitudinal directions were gone through to take the side imaging around Bent 2.

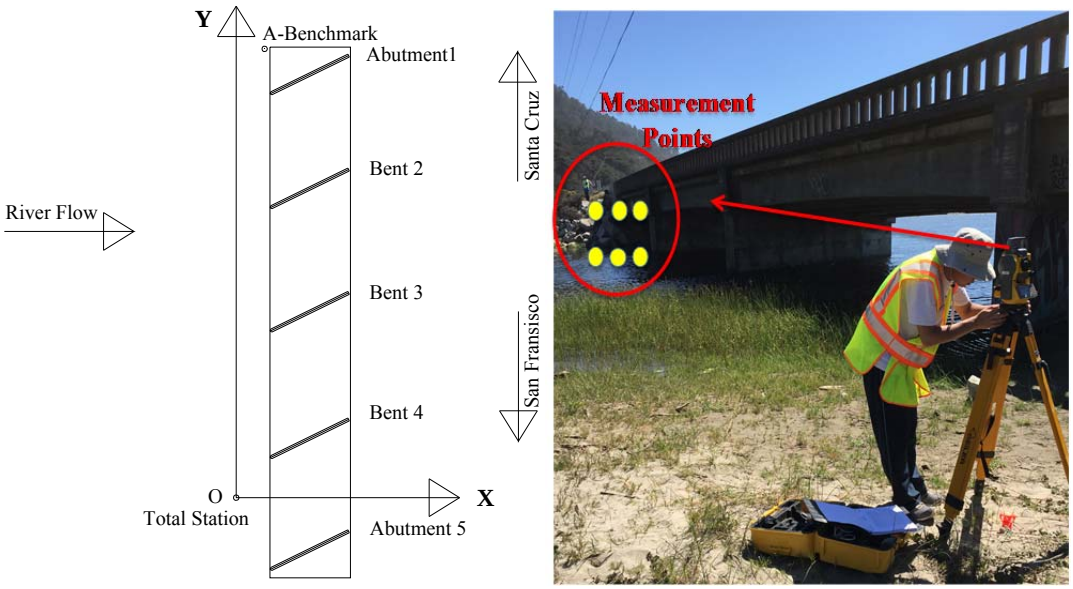

Figure 6 The Coordinate System Selection

(a) Sonar Instrument (b) Operation on the Boat

Figure 7 Riverbed Profiling with a Sonar Instrument

Figure 8 shows the transverse and longitudinal sections of the riverbed profile near Pier 2. Reading from Figure 8, a significant scour hole has been developed around Pier 2 with the maximum water depth of about 7 ft. The actual water depth could be deeper than 7 ft since the boat was unable to pass through very close to the bridge pier. From the longitudinal cross section, it can be determined that the scour hole has been developed on both sides of Pier 2. Therefore, two smart rocks were deployed at the two sides to monitor further evolvement of the scour hole.

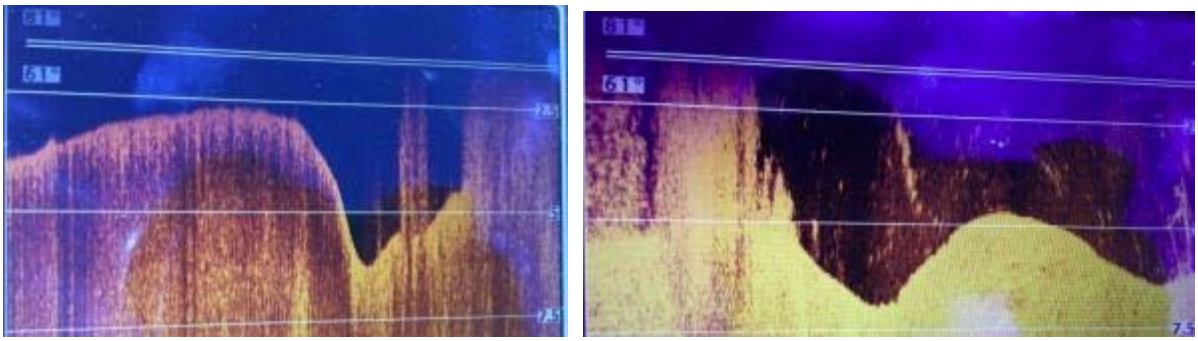

(a) Transverse Section (b) Longitudinal Section

Figure 8 Cross Section of Riverbed around Pier 2

(3) ***Assemble the Test Apparatus***. As shown in Figure 9, the test apparatus is composed of five components. Comp. 1 is a horizontal bar made of aluminum alloy to support the sensor and prisms. Comp. 2 is a modular section of up to 10 pieces made of carbon fiber tube to extend the measurement points downward from bridge deck to the area close to the deployed smart rocks. Comp. 3 is a horizontal outrigger made of aluminum alloy to extend the measurement points away from the bridge deck. It consists of five pieces, each being 1.2 m long. Comp. 4 is a manual forklift made of steel to allow up and down movement of the sensor during field tests. It is supported on four wheels that can move in any direction in the horizontal plane. Comp. 5 represents steel plates as extra weights to balance the forklift during operation. To expedite the assembling process, the five pieces of Comp.3 were first connected and tightened by cables. The Comp. 3 was then placed on the forklift with balanced weights. Next, one piece of 1.0 m long carbon tube was attached to the Comp. 3 and joined by additional carbon tubes as needed for a particular test. Finally, Comp. 1 with the sensor and prisms mounted was connected to the end of Comp. 2 as shown in Figure 5(b).

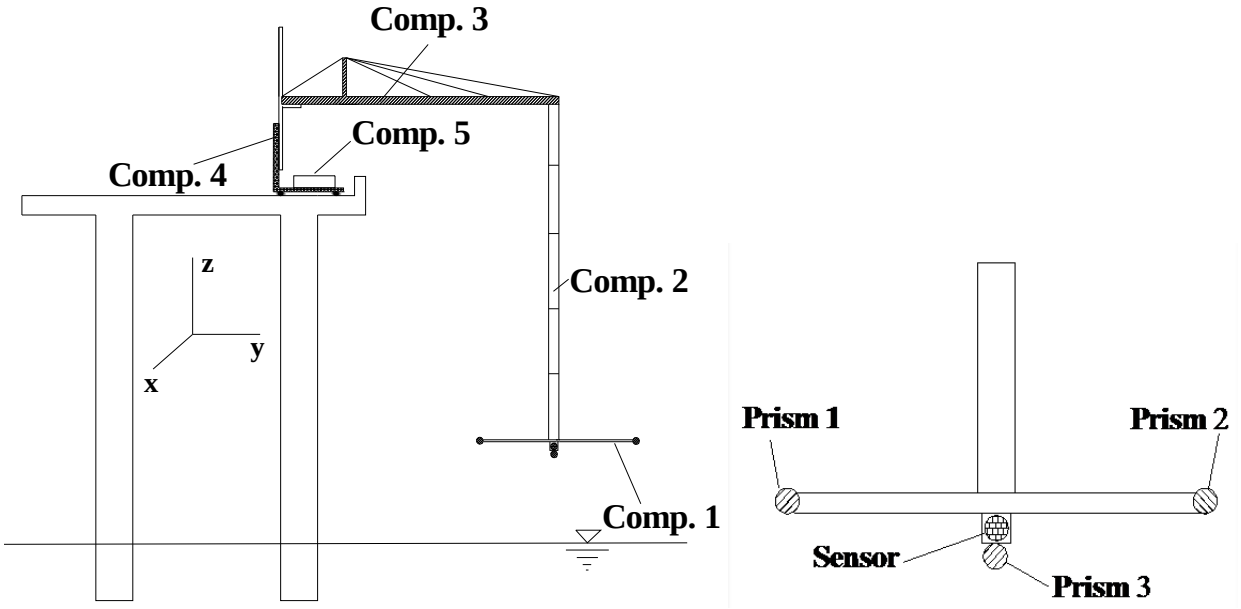

Figure 9 Schematic View of the Test Apparatus

(4) ***Set up the STL Digital Magnetometer***. As shown in Figure 10, a cable was used to connect the sensor to the interface which was powered by a commercial power box with rechargeable battery. The interface was also connected to the laptop by an Ethernet cable. The custom-made software installed in the laptop computer, provided by the manufacturer of the magnetometer system, controlled all measurements during tests.

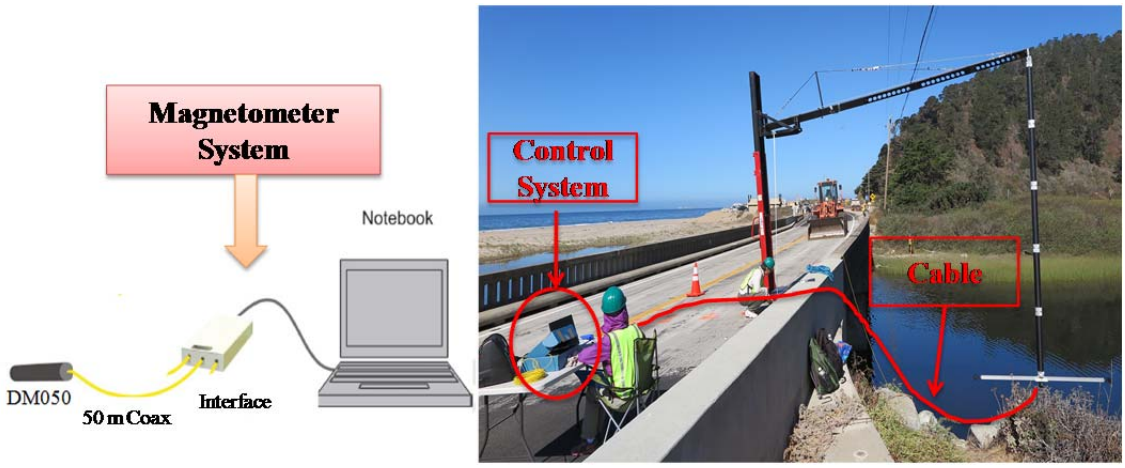

Figure 10 The Magnetometer System Set-up

(5) ***Measure the Ambient Magnetic Field (AMF)***. The ambient magnetic field is generated by the Earth and nearby ferromagnetic objects. It was measured prior to the deployment of smart rocks. Because of limited time, field measurements around the south abutment were taken only at Y1, Y2, and Y3 in Y direction; X1, X2, X3 and X4 in X direction; and Z1, Z2,..., Z7 in Z direction. At Bent 2, Y1, Y3 and Y5 were selected in Y direction, four movements along X-axis and seven movements along Z-axis were considered. As shown in Figure 11(a), the forklift was first placed at Y1X1 and lowered down, taking measurements from Z1 to Z7 or Z7 to Z1. At each Z level, the coordinate and intensity were collected simultaneously as shown in Figure 11(b). After finishing seven levels at Y1X1, the forklift was moved to Y1X2, Y1X3 and Y1X4 to take the measurement successively along X axis. Then, move the forklift to Y2 and Y3 lines to repeat the same procedures as that of Y1X1 for south abutment. The same steps were repeated for Bent 2 to complete the measurement along the lines of Y1, Y3 and Y5. The entire measurement sequence for Abutment 1 and Bent 2 is listed in Figure 11(c).

(a) Test Apparatus Located at Y1X1

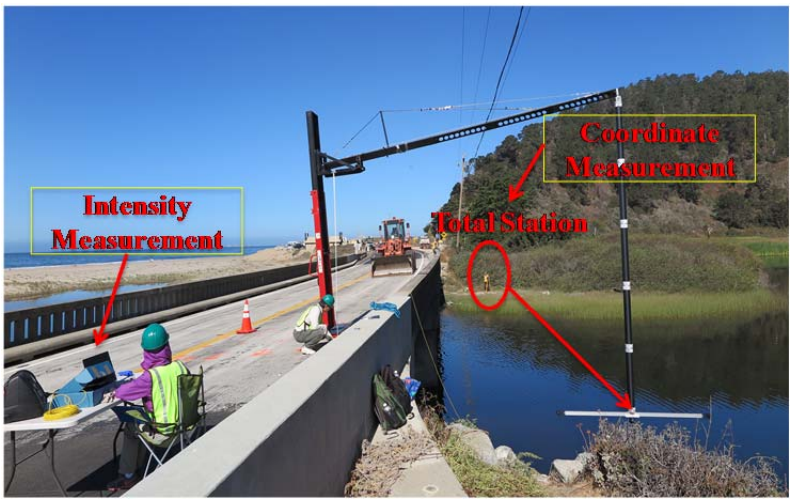

(b) Coordinate and Intensity Measurement

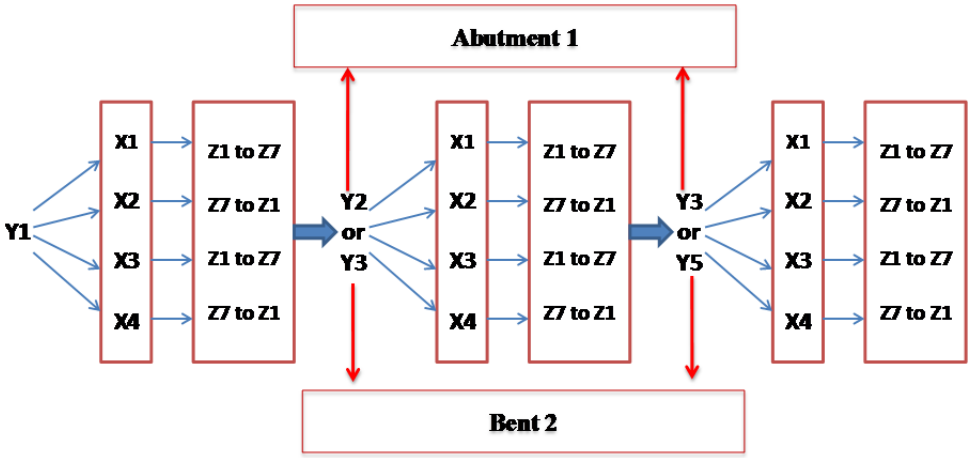

(c) Measurement Point Sequence Arrangement

Figure 11 Arrangement of Ambient Magnetic Field Measurement

(6) ***Deploy Smart Rocks***. As shown in Figures 12(a) and 12(b), the smart rocks SR1 and SR2 were located around Pier 2 for scour monitoring and SR3 between two rocks around the south abutment for riprap measure effectiveness monitoring. The three smart rocks were individually transported in a boat from the downstream river bank and deployed at the predetermined sites. Figure 12(c) shows the deployed smart rocks. SR3 can be easily seen from the bridge deck, SR 2 was also visible without wind, and SR3 was pretty close to the bottom of scour hole with the rope floated on the water surface.

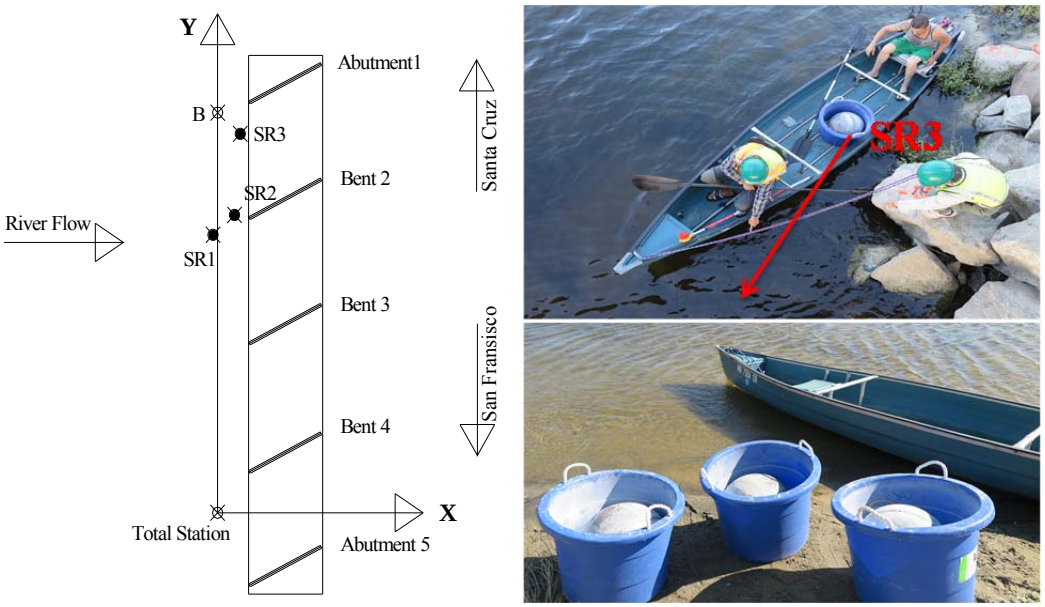

(a) Schematic View of Smart Rock Locations (b) Deployment of SR3

(c) Deployed Smart Rocks
Figure 12 Deployment of Smart Rocks

(7) ***Measure the Coordinates of Smart Rocks***. The coordinates of three smart rocks were measured with the total station through the prism placed on each smart rock.

(8) ***Measure the Total Magnetic Field***. After the deployment of smart rocks, the total magnetic field from the smart rocks, the Earth, and the nearby ferromagnetic objects was measured following the same procedure as used for the AMF measurements except that the movement in Z direction was 6 levels for all points in Mesh 2. Therefore, the total measurement points were 72

and 84 around the south abutment for SR3 and around Bent 2 for SR1 and SR2, respectively. Figure 13 shows two measurements of Y1X1Z7 and Y1X4Z1 above the SR3.

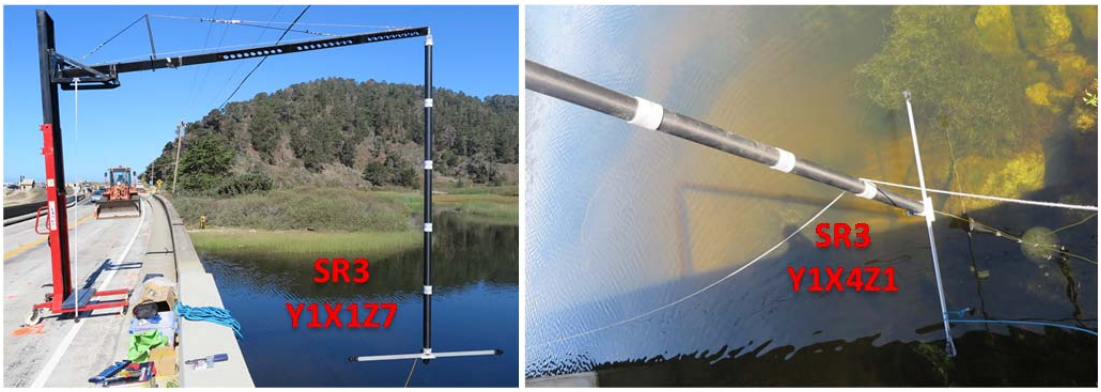

Figure 13 Measurement Conducted above SR3

C. River Bank Measurement around South Abutment

As indicated in Figure 14, measurements were also taken along the river bank. Ten points were selected and marked by the spraying paint on rocks as part of the scour countermeasure around the abutment. Two levels in Z direction were realized by moving up and down a pole with the attached sensor. The coordinates of the sensor locations were all measured with the total station through the prism placed at each point. The ambient magnetic field at 18 points was measured before the placement of the smart rock SR3. The total magnetic field at the 18 points was also collected after deployment of the smart rock SR3.

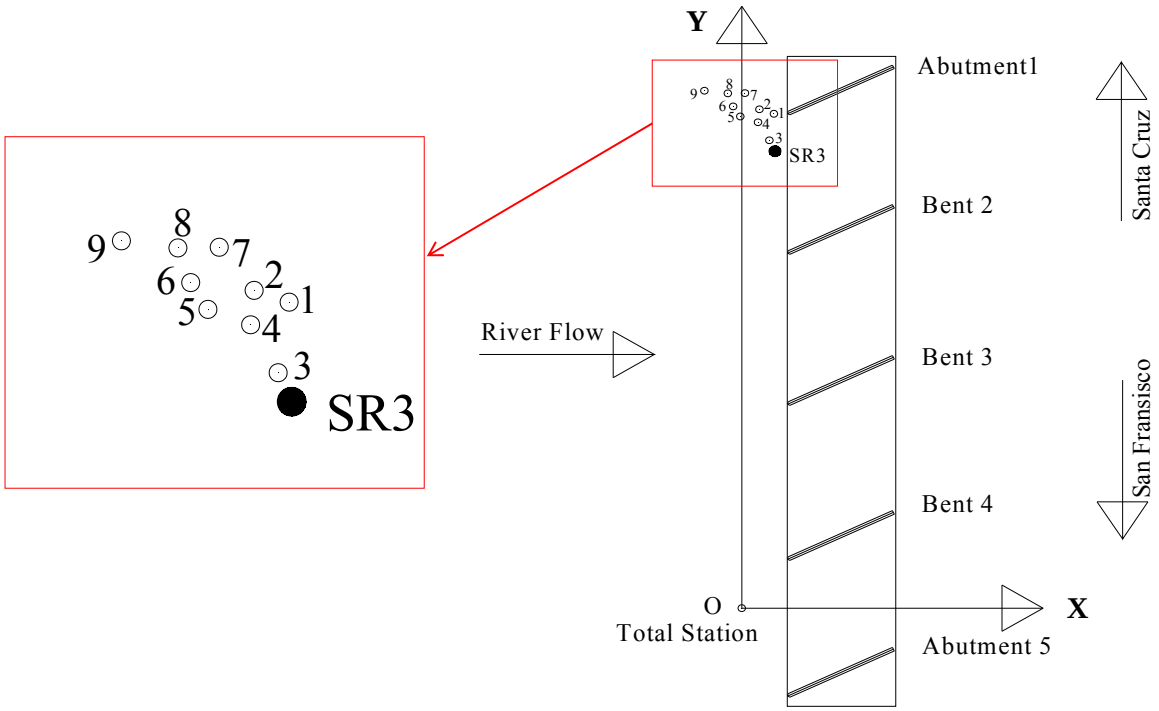

Figure 14 Measurement Points at River Bank

D. Localization Algorithm

Eqs. (1) to (4) represent the relationship among the total magnetic field intensity (B), the ambient magnetic field (B_{XA}, B_{YA} and B_{ZA}), and the magnetic field of a smart rock at coordinates (X_M, Y_M, Z_M), which were measured at each point with coordinates (X,Y, Z). The objective error function expressed into Eq. (5) was minimized through an appropriate optimization algorithm to numerically solve for the location of the smart rock. Note that the local coordinate system xyz parallel to the global XYZ system is set at the location of the smart rock.

$$B = \sqrt{(B_{XM} + B_{XA})^2 + (B_{YM} + B_{YA})^2 + (B_{ZM} + B_{ZA})^2} \tag{1}$$

$$\begin{pmatrix} B_{XM} \\ B_{YM} \\ B_{ZM} \end{pmatrix} = \mathbf{T}^{-1} \begin{pmatrix} -k\dfrac{3zx}{r^5} \\ -k\dfrac{3zy}{r^5} \\ -k\dfrac{(2z^2 - x^2 - y^2)}{r^5} \end{pmatrix} \tag{2}$$

$$r = \sqrt{x^2 + y^2 + z^2} \tag{3}$$

$$x = X - X_M\ ,\ y = Y - Y_M\ ,\ z = Z - Z_M \tag{4}$$

$$J(X_M, Y_M, Z_M) = \sqrt{\sum_{i=1}^{n} [B_i^{(P)} - B_i^{(M)}]^2} \tag{5}$$

E. Test Results and Discussion

Table 1 summarizes the coordinates of 18 measurement points, the AMF intensities prior to deployment of smart rocks, and the total intensities after deployment of the smart rock SR3. The coefficient K for the N42 magnet is calculated from the maximum residual flux density. The three components of the total magnetic field (B_x, B_y, B_z) were directly measured from the 3-axis flux magnetometer in which three directions marked on the sensor was placed exactly parallel to the three axles of the O-XYZ coordinate system. Therefore, the three components of the total magnetic field and the three components (B_{Ax}, B_{Ay} and B_{Az}) of the ambient magnetic field were substituted into the localization algorithm to determine the coordinates of the smart rock SR3.

Table 2 compares the predicted and measured coordinates (X_M,Y_M, Z_M) of the smart rock SR3. Their differences are evaluated in component and the total field intensity as shown in Table 2. It can be observed that the largest error in Z coordinate is 29.6 cm as result of the fluctuation of the sensor caused by the strong wind. The SRSS prediction error of three components is 36.4 cm, which is quite small in comparison with the error limit of half a meter.

Table 1 Coordinates and Intensities of Measurement Points on Bridge Deck for SR3

		Measurement Point Coordinate (m)			N42 Magnet Factor ($nT.m^3$)	AMF Intensity (nT)				SR3 & AMF Intensity (nT)			
		X_i	**Y_i**	**Z_i**	**K**	**B_{Ax}**	**B_{Ay}**	**B_{Az}**	**B**	**B_x**	**B_y**	**B_z**	**B**
Y1X2	Z1	0.656	42.259	-0.942	86521	-18675	-9823	-40007	45230	-17485	-6252	-41897	45828
	Z2	0.686	42.288	-0.638	86521	-18669	-9738	-40124	45313	-18204	-6876	-41683	46001
	Z3	0.703	42.300	-0.318	86521	-18651	-9802	-40170	45360	-18622	-7310	-41496	46067
	Z4	0.703	42.251	-0.026	86521	-18660	-9745	-40236	45411	-19111	-7060	-41313	46064
	Z5	0.751	42.252	0.277	86521	-18719	-9736	-40241	45436	-19666	-7233	-40995	46040
	Z6	0.768	42.345	0.573	86521	-18661	-9888	-40226	45433	-19943	-7237	-40802	45988
Y1X3	Z1	1.693	42.293	-1.141	86521	-18243	-9707	-39974	45000	-13343	-8111	-48963	51393
	Z2	1.753	42.302	-0.840	86521	-18284	-9664	-40184	45193	-16005	-6751	-47086	50188
	Z3	1.684	42.248	-0.537	86521	-18403	-9694	-40314	45364	-17013	-6125	-45233	48713
	Z4	1.685	42.272	-0.245	86521	-18505	-9692	-40438	45514	-18082	-6588	-44021	48044
	Z5	1.708	42.276	0.056	86521	-18708	-9591	-40517	45647	-18927	-6588	-43154	47581
	Z6	1.736	42.275	0.366	86521	-18878	-9675	-40509	45727	-19475	-7190	-42452	47256
Y1X4	Z1	2.341	42.387	-1.085	86521	-16406	-10804	-40258	44795	-13358	-11669	-54780	57580
	Z2	2.341	42.371	-0.885	86521	-16560	-10632	-40585	45104	-14736	-9244	-52073	54901
	Z3	2.378	42.337	-0.586	86521	-16763	-10553	-40843	45393	-16360	-8080	-48899	52193
	Z4	2.381	42.291	-0.283	86521	-16969	-10624	-41047	45670	-17499	-7475	-46705	50433
	Z5	2.424	42.336	0.015	86521	-17321	-10588	-41205	45934	-18186	-7539	-45310	49402
	Z6	2.444	42.329	0.319	86521	-17707	-10784	-41228	46147	-18941	-7994	-44345	48879

Table 2 Predicted and Measured Location of Smart Rock SR3 Based on Measurements on Bridge Deck

	X_M/m	Y_M/m	Z_M/m
Predicted SR3 Location	2.789	41.302	-2.823
Measured SR3 Location	2.714	41.104	-2.527
Location Prediction Error for SR3	0.075	0.198	-0.296
SRSS Error in Coordinate	0.364		

Similarly, Table 3 summarizes the coordinates and magnetic intensities at 18 measurement points collected from the river bank around the south abutment. The same localization algorithm was adopted to calculate the coordinates of the SR3, designated as predicted SR3 location, displayed in Table 4. The ground true coordinates of SR3 surveyed from the total station designated as measured SR3 location is also shown in Table 4. It is observed that the location prediction errors for SR3 in Y and Z coordinates are 27.9 cm and 19.7 cm, which are acceptable compared to the half a meter limit. However, the error of X coordinate is 52.8 cm which is a little beyond the half meter limit because that the X, Y, Z axis on the sensor cannot be guaranteed to perfectly parallel to that of the coordinate system of the total station. The angle between X axis

on the sensor and that of the total station leads to the larger error of the X-component of the ambient magnetic field. Therefore, the SRSS error exceeds the half meter limit.

Table 3 Coordinates and Intensities of Measurement Points for SR3 from River Bank

Point Name	Measurement Points Coordinate (m)			N42 Magnet Factor ($nT.m^3$)	AMF Intensity (nT)			SR3 & AMF Intensity (nT)
	X_i	Y_i	Z_i	K	B_{XA}	B_{YA}	B_{ZA}	B
N1	2.627	44.468	0.288	86521	24093	7690	-37484	45217
N2	2.627	44.468	2.088	86521	23731	5492	-38171	45281
N3	1.440	44.867	0.013	86521	18165	11472	-38890	44430
N4	1.440	44.867	1.813	86521	17163	10703	-39064	43990
N5	2.255	42.083	-1.258	86521	16476	12982	-39401	44637
N6	2.255	42.083	0.542	86521	18764	11114	-40416	45925
N7	1.324	43.703	-0.832	86521	18524	11451	-39087	44744
N8	1.324	43.703	0.968	86521	18011	12356	-39613	45235
N9	-0.122	44.223	-1.594	86521	17208	14716	-38936	45040
N10	-0.122	44.223	0.206	86521	17466	13609	-39242	45058
N11	-0.706	45.130	-1.236	86521	18448	13334	-39060	45208
N12	-0.706	45.130	0.564	86521	18635	12269	-39233	45133
N13	0.260	46.324	0.062	86521	12898	15931	-39174	44212
N14	0.260	46.324	1.862	86521	16874	12596	-39219	44514
N15	-1.139	46.302	-0.897	86521	18671	12589	-39042	45071
N16	-1.139	46.302	0.903	86521	19428	10628	-39302	45112
N17	-3.051	46.542	-1.454	86521	19565	10776	-39301	45205
N18	-3.051	46.542	0.346	86521	19490	11350	-40115	46021

Table 4 Predicted and Measured Location of SR3 from River Bank

	X_M/m	Y_M/m	Z_M/m
Predicted SR3 Location	3.317	41.581	-2.626
Measured SR3 Location	2.789	41.302	-2.823
Location Prediction Error for SR3	0.528	0.279	-0.197
SRSS Error in Coordinate	0.628		

Task 3.2 Visualization Tools for Rock Location Mapping over Time

This task will not start till the 5th quarter.

Task 4 Technology Transfer, Report and Travel Requirements

The 4st quarterly report is being submitted.

I.2 PROBLEMS ENCOUNTERED

In this quarter, smart rock deployment was postponed due to delayed manufacture and shipping of the test apparatus.

I.3 FUTURE PLAN

The following task and subtasks will be executed during the next quarter.

Task 3.1 Time- and Event-based Field Measurements

The field tests at bridge sites in Missouri will be conducted to validate the localization algorithm of smart rocks.

Task 3.2 Visualization Tools for Rock Location Mapping over Time

This task will not start till the 5th quarter.

Task 4 Technology Transfer, Report and Travel Requirements

The 5th quarterly report will be prepared and submitted.

II – BUSINESS STATUS

II.1 HOURS/EFFORT EXPENDED

The planned hours and the actual hours spent on this project are given and compared in Table 5. In the fourth quarter, the actual hours are less than the planned hours, leading to an actual cumulative hour of approximately 42% of the planned hours. The cumulative hours spent on various tasks by personnel are presented in Figure 15.

Table 5 Hours Spent on This Project

	Planned		Actual	
	Labor Hours	Cumulative	Labor Hours	Cumulative
Quarter 1	945	945	176	176
Quarter 2	752	1697	294	471
Quarter 3	752	2449	294	765
Quarter 4	752	3202	566	1331
Quarter 5				
Quarter 6				
Quarter 7				
Quarter 8				

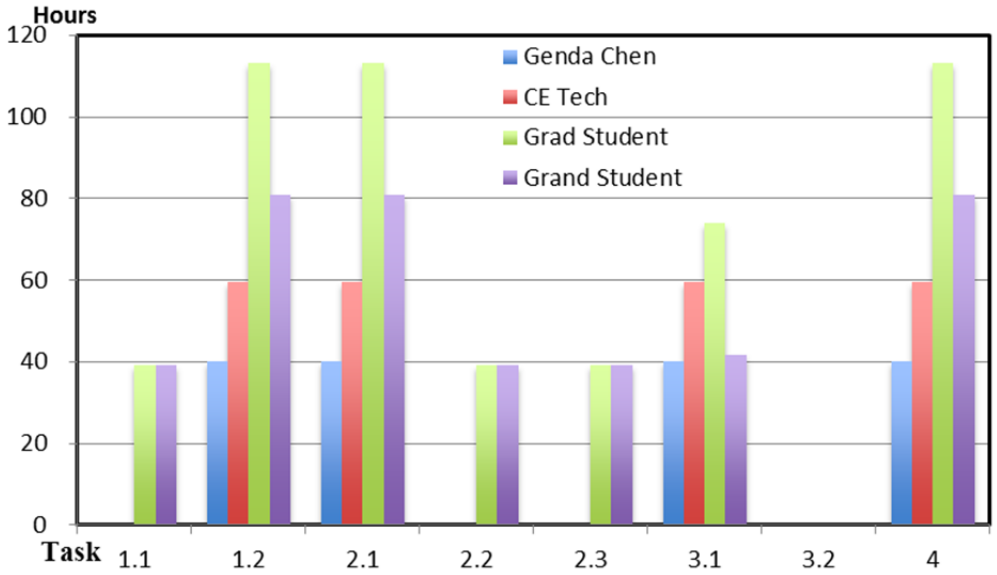

Figure 15 Cummulative Hours Spent on Various Tasks by Personnel

II.2 FUNDS EXPENDED AND COST SHARE

The budgeted and expended OST-R funds accumulated by quarter are compared in Figure 16. Approximately 108% of the budget has been spent till the end of fourth quarter. The actual cumulative expenditures from OST-R and MS&T/MoDOT are compared in Figure 17. The expenditure from OST-R is slightly over the combined amount from the MS&T and MoDOT.

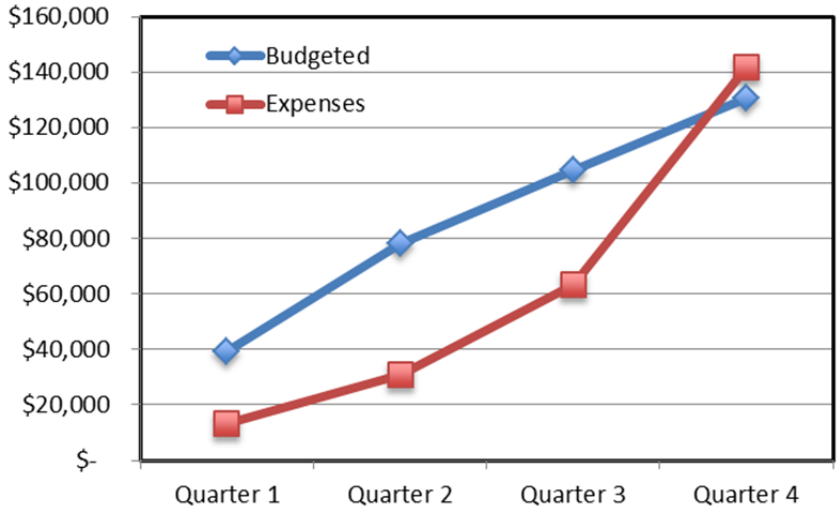

Figure 16 Comparison of OST-R Budget and Expenditure Accumulated by Quarter

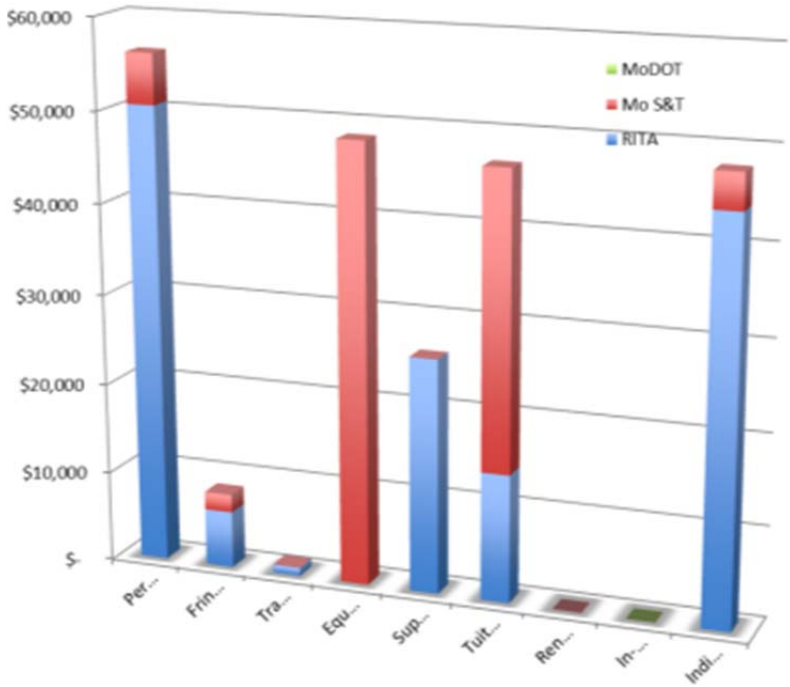

Figure 17 Cummulative Expenditures by Sponsor